Iranian Journal of Oil & Gas Science and Technology, Vol. 9 (2020), No. 4, pp. 1–28
http://ijogst.put.ac.ir

Seismic Attribute Analysis and 3D Model-Based Approach to Reservoir Characterization of "KO" Field, Niger Delta

Abe Sunday James[1*] and Okosun Kenneth Olayinka[2]

[1] Ph.D. , Department of Applied Geophysics, Federal University of Technology, Akure, Nigeria
[2] B. Tech., Department of Applied Geophysics, Federal University of Technology, Akure, Nigeria

Highlights

- Seismic, check-shot, and well logs data are analyzed for the reservoir characterization and modeling of "KO" Field in Niger Delta.
- Interpretation of the well logs is matched to the seismic lines to ensure that there is a good correlation between them.
- Three different seismic attributes are used to identify high amplitude regions and to perform a comprehensive structural interpretation of the field.
- A geological model representing the structural, stratigraphic, lithological, petrophysical features of the reservoir is constructed and evaluated.

Received: May 28, 2020; *revised*: August 03, 2020; *accepted*: August 07, 2020

Abstract

Modelling involves the use of statistical techniques or analogy data to infill the inter-well volume producing images of the subsurface. The integration of available data sets from "KO" field was used to identify hydrocarbon prospects and, by means of interpolation, populate the facies and petrophysical distribution across the field to define the reservoir properties for regions with missing logging data. 3D seismic data, check-shot data, and a series of well logs of four wells were analyzed, and the analysis of the well logs was performed using the well data. The synthetic seismogram produced from the well ties was used to map horizon slices across the reservoir regions. Four horizons and 15 faults, including one growth fault, four major faults, and other minor faults, all in the time domain were mapped. Attribute analyses were carried out, and a 3D static model comprised of the data from the isochore maps, faults, horizons, seismic attributes, and the various logs generated was built. A stochastic method was also employed in populating the facies and petrophysical models. Two hydrocarbon-bearing sands (reservoirs S1 and S2) with depth values ranging from –1729 to 1929 m were mapped. The petrophysical analysis gave porosity values ranging from 0.18 to 0.24 across the reservoirs, and the permeability values ranged from 2790 to 5651 mD. The water saturation (S_w) of the reservoirs had an average value of 50% in reservoir S1 and 47% in reservoir S2. The depth structure maps generated showed an anticlinal structure in the center of the surfaces, and the mapped faults with the four wells were located in the anticlinal structure. The reserve estimate for the stock tank oil initially in place (STOIIP) of the reservoirs was about 70 mmbbl, and the gas initially in place (GIIP) of the reservoirs ranged from 26714 to 63294 mmcf. The result of the petrophysical analysis revealed the presence of hydrocarbon at favorable quantities in the wells, while the model showed the distribution of these petrophysical parameters across the reservoirs.

Keywords: Reservoir Characterization, Seismic Attributes, 3D Static Modeling

* Corresponding author:
Email: jsabe@futa.edu.ng

How to cite this article
Sunday James A, Kenneth Olayinka O, Seismic Attribute Analysis and 3D Model-Based Approach to Reservoir Characterization of "KO" Field, Niger Delta. Iran J. Oil Gas Sci. Technol., Vol. 9, No. 4, p. 1–28, 2020.
DOI: http://dx.doi.org/10.22050/ijogst.2020.232984.1550

1. Introduction

Understanding reservoir characteristics is a crucial factor in quantifying producible hydrocarbons (Schlumberger, 1989). For reservoir characterization, the results obtained from the previous studies such as regional geology, seismic imaging, and well data analyses, are all combined. The information on the reservoir rock behavior and the fluid in place obtained from reservoir characterization studies must be sufficient to build a 3D geological model of the reservoir zone. This model is where all the data and interpretation results are integrated into a consistent understanding of the reservoir.

Cosentino (2001) emphasized the relevance of a sound geological model in the overall reliability of a reservoir study, stating that the static description of the reservoir, both in terms of geometry and petrophysical properties, is one of the main controlling factors in determining the field production performance.

The main objective of reservoir characterization studies is to identify the heterogeneities of the reservoir rock. These heterogeneities are spatial geological variations on different scales, which can modify the fluid movement inside the reservoir. A seismic attribute is a measurement derived from seismic data (Mickaele et al., 2014). Seismic attributes are mathematical descriptions of the geometry/shape or other characteristics of a seismic trace over specific time intervals, and they reveal the features and patterns that otherwise could not be detected.

Seismic attributes have been increasingly used in both exploration and reservoir characterization studies and routinely been integrated into the seismic interpretation processes (Partyka et al., 1999). Further, the analyses of the attribute of the seismic data can boost the quantity and quality of the data (Herrera et al., 2006). These attributes enable interpreters to extract more information from the seismic data.

The applications of attribute analyses include hydrocarbon play evaluation, prospect identification and risking, reservoir characterization, well planning, and field development. There are different classes of seismic attributes based upon the nature of estimation and the property of the reservoir.

This study integrates the seismic attribute analyses with petrophysical interpretation, which will help delineate the subsurface structures that are favorable for the accumulation of hydrocarbon. A sequential workflow is designed for seismic interpretation and attribute mapping to identify fracture, horizon continuity, stratigraphy, facies, and potential prospects. The geologic model will present a true image of the reservoir within the subsurface and give an idea of how the petrophysical properties are distributed spatially within the reservoir; it also determines the interconnectivity of the reservoirs within the field.

The results of this research, which include the petrophysical characteristics of the reservoirs and a 3D geologic model, are no doubt rich enough to be used to estimate the hydrocarbon quality and potential in the studied area. They will also help enhance our knowledge about how to construct a geological model for future dynamic modeling as a tool for field performance monitoring.

1.1. Aim and objectives

This study aims to identify potential hydrocarbon prospects while defining and visualizing the geological properties across the reservoirs present in the "KO" field, Niger Delta using seismic attributes and a 3D static reservoir model.

The objectives of this work include:

- identifying and delineating potential reservoirs and hydrocarbon horizon useful for field development and the location of best productive zones for future wells in the field;
- determining which seismic attribute analysis is applicable to the KO field;
- estimating petrophysical parameters such as porosity, permeability, net-to-gross, and hydrocarbon saturation of the reservoirs in the field;
- determining the fluid types and contacts in the reservoirs;
- estimating the pore volume of the hydrocarbon of the reservoirs.

1.2. Location and geology of the study area

The KO field is located within the Niger Delta province as shown in Figure 1. It is a shallow offshore field located in Bayelsa state, Nigeria, lying at a latitude of 04° 8' 48.606" and a longitude of 05° 58' 40.523". The name given to this field and the well headers are fictitious and only valid in this work.

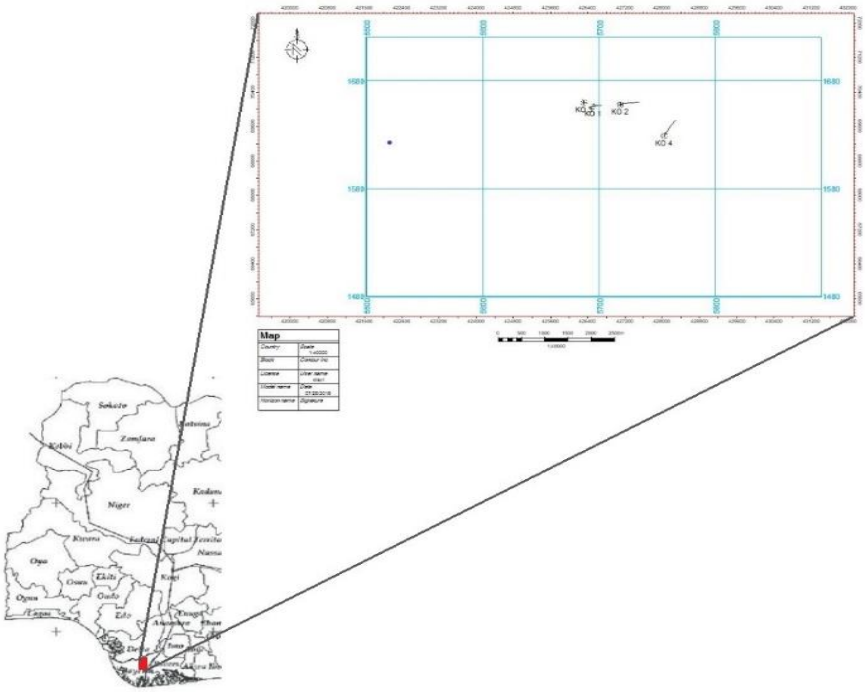

Figure 1

The location and base map of the study area.

The Niger Delta region is situated in the Gulf of Guinea at a longitude of 5ºE to 8ºE and a latitude of 4ºN to 6ºN. The onshore portion of the Niger Delta Province is delineated by the geology of southern Nigeria and southwestern Cameroon. The northern boundary is the Benin flank, an east–northeast trending hinge line in the south of the West Africa basement massif. The northeastern boundary is defined by outcrops of the Cretaceous on the Abakaliki High and further in the east–southeast by the Calabar flank, a hinge line bordering the adjacent Precambrian. The offshore boundary of the province is defined by the Cameroon volcanic line to the east, the eastern boundary of the Dahomey Basin (the eastern-most West African transform-fault passive margin) to the west, and the two-kilometer sediment thickness contour or the 4000 meter bathymetric contour in areas where the sediment thickness is greater than two kilometers to the south and southwest (Tuttle et al., 1999).

The Niger Delta Basin was formed in the site of a triple-point junction related to the opening of the southern Atlantic starting in the Late Jurassic and continuing into the Cretaceous. The delta proper began developing in the Eocene. It is one of the largest deltas in the world with an area of approximately 300,000 km², a sediment volume of 500,000 km³, and a sediment thickness of over 10 km in the basin depo-center. The province covers 300,000 km² and includes the geologic extent of the Tertiary Niger Delta (Akata–Agbada) petroleum system (Tuttle et al., 1999). The Niger Delta province contains only one identified petroleum system which is referred to as the Tertiary Niger Delta (Akata–Agbada) petroleum system.

Three major lithostratigraphic formations are recognized in the Niger Delta: the Benin, Agbada, and Akata formations. The Agbada formation, which is the major oil-producing formation in the Niger Delta Complex Basin, is characterized by paralic interbedded sandstone and shale with a thickness of over 3000 m (Reijers, 1996). These paralic clastics are the truly deltaic portion of the sequence and were deposited in a few delta-front, delta-topset, and fluvio-deltaic environments. Some shales of the Agbada formation were thought to be the source rocks; however, Ejedawe et al. (1984) deduced that the main source rocks of the Niger Delta are the shales of the Akata formation. As with the marine shales, the paralic sequence is present in all depobelts and ranges in age from the Eocene to the Pleistocene.

2. Materials and methodology

The materials used for this study include:

- A 3D seismic data set (SEGY);
- A well header;
- A series of well logs for the four wells (KO 1, KO 2, KO 3, KO 4);
- Well deviation data (ASCII);
- Check-shot data;
- Petrel 2015 software.

Figure 2 illustrates the workflow of this research, which was carried using Petrel software. The quality check of the given data is carried out, which involves checking seismic and well log data, viewing the data format, survey geometry, and making sure they are all from the same field. After the quality and quantity of the data set are found to be satisfactory for the objective of the study, the data are imported into the software for interpretation.

The SEGY seismic data set used for this study was imported into a user-defined folder. The well data are loaded into Petrel by first creating a well folder and importing the well header which allows the display of well position on the base map. The well header in the ASCII format contains information on:

- the well name;
- unique well identifier;
- surface X and surface Y;
- Kelly bushing (well datum value);
- total depth (measured depth).

The well logs (LAS format), the well deviation (ASCII format), and the check-shot data on each well are imported into the well folder.

The method adopted to achieve the highlighted objectives includes the delineation of lithologies and the identification of the reservoirs from the signatures of gamma-ray logs and resistivity logs. Table 1 lists the available composite logs used in this study. For this research, three tracks named track I, track

II, and track III are used in presenting the well log. Track I is a linear scale with 10 standard divisions of 0.25 inch and is a 0.75 inch span (on which the depth is printed) containing the gamma-ray logs on a scale in the range of 0–150 gAPI increasing from left to right. Track II, on the other hand, is a logarithmic scale having four-cycle samples containing the induction log in a scale range of 0.2 to 2000 Ωm. Track III is a split grid holding the neutron-porosity log (NPHI) and the density log (RHOB). The scale of the density log ranges from 1.65 to 2.65 gcm³, while the neutron-porosity is reversed in a scale range of 0 to 60 m³.

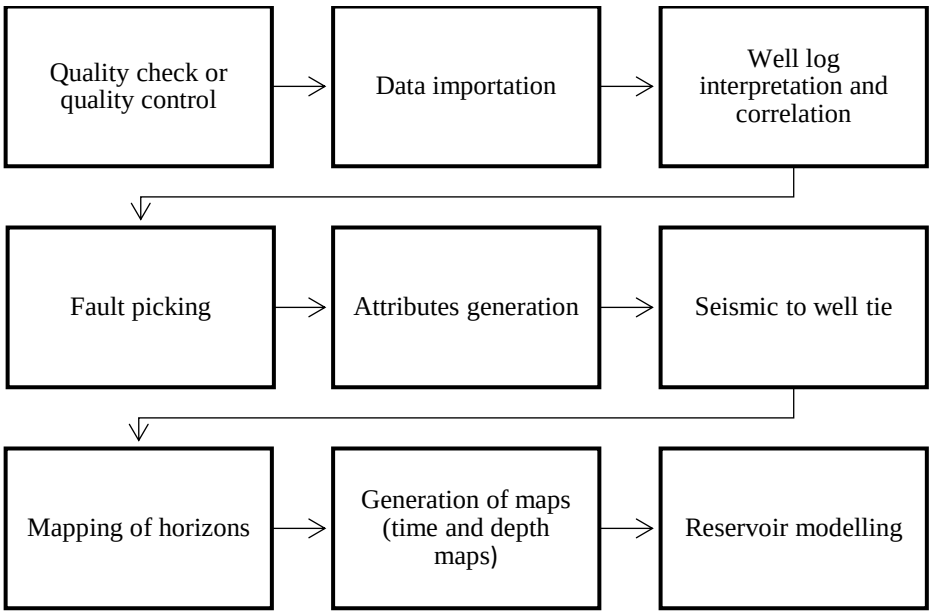

Figure 2

Integrated workflow of the reservoir characterization of the KO field.

Table 1

The logs utilized in this study.

Name	KO 1	KO 2	KO 3	KO 4		
Deviation survey	•	•	•	•		
Caliper	•	•	•	•		
Sonic	•	x	•	•		
Gamma ray	•	•	•	•		
Neutron	•	•	•	•		
Density	•	•	•	•	Key	
Resistivity	•	•	•	•	•	Available
Check-shot	x	x	x	•	x	Not available

The petrophysical parameters evaluated in this study include volume of shale, porosity, permeability, hydrocarbon saturation, and water saturation.

2.1. Volume of shale (V_{sh})

Gamma ray log is used to estimate the volume of shale. The relationship between the magnitude of the gamma ray and the shale content may be linear or nonlinear. The linear gamma ray–clay volume relationship is used herein:

$$V_{sh} = I_{GR} \tag{1}$$

where I_{GR} is the gamma ray index defined as:

$$I_{GR} = (GR_{log} - GR_{clean})/(GR_{shale} - GR_{clean}) \tag{2}$$

where GR_{log} is log reading at the depth of interest, GR_{clean} represents the gamma ray value in a nearby clean zone, and GR_{shale} stands for the gamma ray value in a nearby shale. I_{GR} describes a linear response to the shaliness or the clay content.

2.2. Porosity (ϕ)

Porosity is the ratio of the pore space in the net reservoir rock; it is therefore a key factor in quantifying oil and gas reserves. It is often represented by ϕ and controlled by the grain size distribution, packing, and the subsequent alteration (e.g. diagenesis).

The porosity of the field is estimated using the density log based on the concept of Wyllie time average equation:

$$\rho ma = \rho b(1 - \phi) + \rho f(\phi) \tag{3}$$

which can be rewritten as:

$$\phi = \frac{\rho ma - \rho b}{\rho ma - \rho f} \tag{4}$$

where ϕ is porosity as derived density, ρma represents the density of the matrix (g/cm^3), ρb is bulk density as derived from the log, ρf stands for the density of the fluid (ρf = 1.0 g/cm^3 for the fresh water muds), and ρf indicates the density of the fluid (ρf = 1.0 g/cm^3 for the fresh water muds).

2.3. Permeability (*K*)

This is a measure of the capacity of a rock pore system to transmit fluid. It is usually determined by the porosity logs and sometimes the cores; an obvious control on permeability is porosity. The larger the pores are, the broader the pathways for fluid flow are. Permeability, unlike the porosity, is a dynamic property and must either be measured dynamically or be inferred.

The method of Wyllie and Rose (1950) for the computation of permeability utilizes the following equations:

$$K^{\frac{1}{2}} = 250(\phi^3/(\text{Swirr})) \qquad \text{(medium gravity oil)} \tag{5}$$

$$K^{\frac{1}{2}} = 79(\phi^3/(\text{Swirr})) \qquad \text{(dry gas)} \tag{6}$$

where *K* is permeability in millidarcies, ϕ represents porosity, *Swirr* indicates the water saturation of a zone at irreducible water saturation. *Swirr* can be calculated using the below equation:

$$Swirr = \sqrt{(F/2000)} \tag{7}$$

where *F* denotes the formation factor and is expressed in:

$$F = a/(\phi m) \tag{8}$$

where *a* represents the tortuosity factor and *m* is the cementation factor. *a* and *m* are constants equal to 0.62 and 2.15 respectively.

The permeability of the formation derived from the wireline logs is restricted to hydrocarbon bearing zones only. The correlation function used for the estimation of the permeability was generated by the least square method as shown below:

The cross-plot of the permeability versus the total porosity (*PERMF* versus *PHIT*) is defined as:

$$Y = (53209.5 \times X) - 7965.53 \tag{9}$$

2.4. Saturation

Water saturation (S_w) is estimated by the total porosity and the resistivity log (Archie, 1942). It is the volume of water contained in the pore volume of the rock. The remainder of the pore volume is, by definition, occupied by hydrocarbons. Water saturation is controlled by grain size and composition, and smaller pores can more strongly bind water to them. In addition, clays can also bind water; thus, rocks that are rich in clay and have small pores have high water saturation. The rocks that are poor in clay and have large pores have the potential to have high hydrocarbon saturation.

$$Sw = \sqrt{(R_w/(ILD \times \phi^{1.74}))} \qquad \text{(Archie, 1942)} \tag{10}$$

where *ILD* is the true resistivity of the formation, and R_w denotes the water resistivity.

The hydrocarbon saturation is the volume of the pore space occupied by hydrocarbons and can be calculated as $1 - S_w$.

Seismic to well tie is done to match the events on well logs to the specific seismic reflections. To enhance the display of the structural features and the hydrocarbon potential of the field, the analysis of the seismic attributes is carried out using one surface attribute and two volume attributes which are cosine of phase, amplitude, and variance method. Fault mapping is performed on the vertical seismic display across the whole seismic volume. Horizons are mapped, auto tracked, and converted to surfaces to obtain the time structure maps. The time structure maps are converted to depth structure maps using the check-shot data provided.

Reservoir modeling is divided into static modeling (geological modeling) and dynamic modeling (flow simulation). In this study, we only take the static reservoir models into account. A static model, also referred to as a geological model, shows the heterogeneity of a formation, that is, the porosity distribution, permeability distribution, and the facies distribution. It is important to note that the static model does not provide the flow pattern of the fluid in the subsurface.

Building a static reservoir model involves the integration of various static data sets including the well data containing the porosity logs (density, neutron, and sonic logs), the permeability logs (from the porosity logs), the facies cutoff (based on the lithologies present in the gamma ray), and the net-to-gross ratio (*N/G*) and saturation (from the resistivity and porosity logs); then, the logs are upscaled and used to populate facies and petrophysical variations in the field. A static model can be grouped mainly into the structural model, stratigraphic model, and lithological/property model.

Structural modeling consists of defining the shape, the volume, and the structural complexity of the studied domain. The primary components are the major horizons and the faults recognized from seismic

picking and time-to-depth conversion (Mickaele et al., 2014). They contribute to the skeleton of the geological grid, the isochore maps, seismic horizons, faults, and seismic attributes are used in building the skeleton of the geological grid.

Under the lithological/property modeling, we consider the facies and petrophysical model. The facies model is useful in the estimation of sediments and understanding of the sedimentary environment. The facies model is computed using the upscaled well logs. The facies log and net-to-gross ratio are used to provide useful information for characterizing the facies.

When the well logs are upscaled, they can be used in deterministic and stochastic modeling. Deterministic techniques are typically used when dense data are available, that is, many wells, and well and seismic data. If no logs are available, deterministic methods cannot be used, and only unconditional stochastic methods and interactive drawing are applicable. Stochastic techniques are often applied under the conditions where sparse data are present. These methods produce a possible result and can be used to produce multiple equally probable realizations.

Because of the sparse well data, the sequential indicator simulation, which is a stochastic technique, is used in this study.

The petrophysical model rests solely on the use of well data for reservoir characterization. The well data also consist of logs and show the porosity, permeability, and water saturation distribution across the reservoir. The Gaussian random function simulation (a stochastic method) is used to generate a model of each property using the upscaled well logs computed by the petrophysical evaluation.

Finally, the hydrocarbon pore volume is estimated, and the volumes are calculated in the volume calculation process step using Petrel software; they are estimated within zones and segments. The contacts defined are used as the input to the volume calculation process.

Formulas utilized by Petrel software for volume computations are expressed by:

$$Net = Bulk\ volume \times N/G \tag{11}$$

$$Pore = Net\ volume \times Porosity \tag{12}$$

$$HCPVo = Pore\ volume \times So \tag{13}$$

$$HCPVg = Pore\ volume \times Sg \tag{14}$$

$$STOIIP = HCPVo/Bo + (HCPVg/Bg) \times Rv \tag{15}$$

$$GIIP = HCPVg/Bg + (HCPVo/Bo) \times Rs \tag{16}$$

$$Recoverable\ oil = STOIIP \times RecFo \tag{17}$$

$$Recoverable\ gas = GIIP \times RecFg \tag{18}$$

where *Bo* represents oil formation volume factor, *Bg* is gas formation volume factor, *Rs* indicates solution gas-to-oil ratio, *Rv* denotes vaporized oil-to-gas ratio, *RecFo* is oil recovery factor, *RecFg* represents gas recovery factor, *GIIP* stands for gas initially in place, and *HCPV* is hydrocarbon pore volume.

3. Results and discussion

3.1. Lithology delineation and well correlation

The general stratigraphy of the four wells in the KO field shows an alternating sequence of sand and shale layers. Nine reservoirs were delineated and correlated across the four wells of KO 1, KO 2, KO 3, and KO 4 in the KO field based on the motif of the gamma ray log. However, this project focused on the characterization of reservoirs S1 and S2.

Reservoir S1 ranges from a depth of 3495 m to a depth of 3616 m. At this level, well KO 3 has no resistivity reading, so it can be stated that it is saturated either with water or with hydrocarbons. Wells KO 1 and KO 2 appear to be saturated with gas, oil, and water as seen from the cross-plot of the neutron log versus the density log, while well KO 4 is saturated with oil.

Reservoir S2 ranges from a depth of 3728 m to a depth of 3901 m. At this level, well KO 3 is saturated with gas, while wells KO 1 and KO 2 appear to be saturated with gas, oil, and water similar to reservoir S1. Well KO 4 can be considered to be wet or completely saturated with water.

3.2. Well log interpretation

The interpretation of the well logs was carried out using the gamma ray logs for lithology delineation and the deep induction logs to determine the fluid type based on the cross-plot of the resistivity and neutron-density for fluid contact. The gamma ray log motif trend was separated into sand and shale units based on their API unit readings. A cutoff was set at 70 API; a reading larger than 70API indicates the shale, while a reading lower than 70API denotes sand. The intercalation of the sand and shale units was therefore spotted across all the wells with similar log signatures; the shale unit appeared to be laterally extensive, while the sand unit had appreciable thickness across the wells. The gamma ray log motif trend was also applied to reservoir S2 so as to interpret its environment of deposition (EOD). It was observed that there was an increase in the gamma ray response, which depicts a fining upward sequence with a sharp base along all the four wells. This suggests that reservoir S2 is becoming rich in clay upwards and may be interpreted as a fluvial, tidal channel.

The hydrocarbon-bearing sands were identified with the aid of the deep induction log and gamma ray, and sands with a high resistivity response were picked out as reservoirs. A cross-plot of the neutron log versus the density logs revealed that the reservoirs were saturated with gas, oil, and water, showing where each of them terminates.

3.3. Well correlation

Correlation exercise was carried out within the given wells of the field to provide a better understanding about the geology of the area and to identify the horizontal sand packages that were deposited at the same time within the field. The wells were correlated along the northwest–southeast direction. From the correlation section shown in Figure 3, it is concluded that the shale layers thin out along the northwest–southeast direction.

Four well tops were created in the stratigraphy folder: S1 TOP, S1 BASE, S2 TOP, and S2 BASE. These well tops were later used to generate isochore points and then isochore thickness maps using the isochore interpolation method. These isochore maps were used in the stratigraphy modeling of the reservoirs.

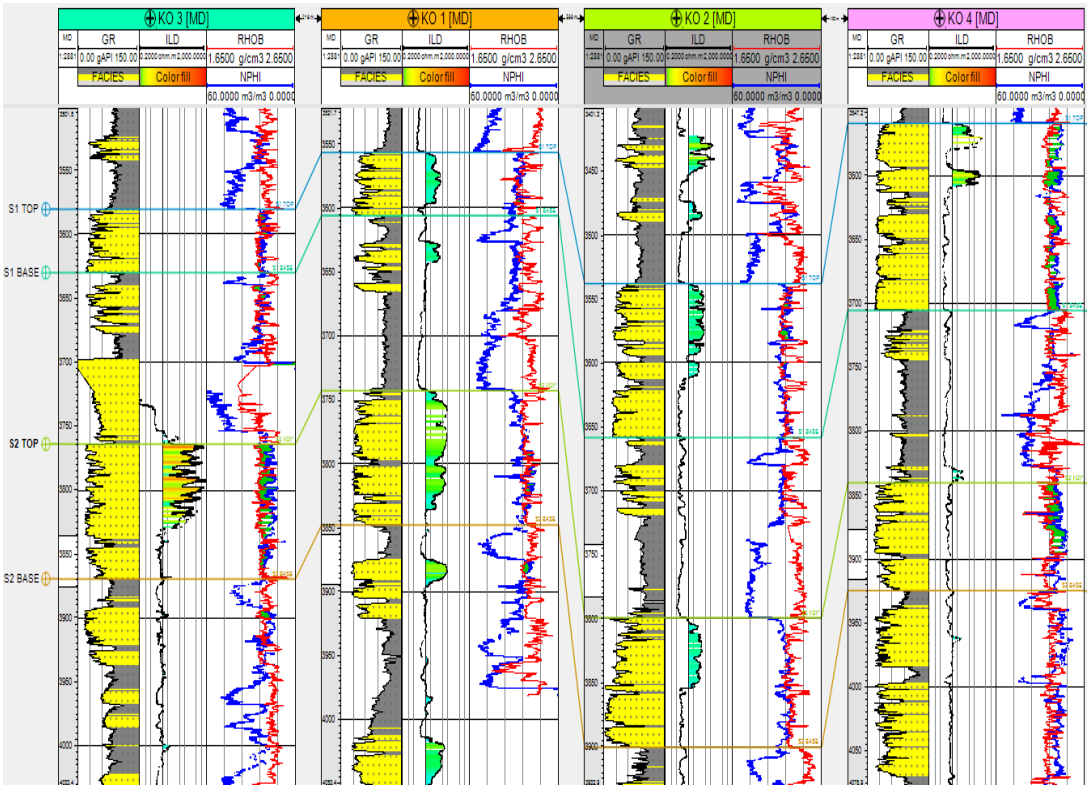

Figure 3

The lithological correlation section of KO field from the northwest–southeast direction.

3.4. Petrophysical analysis

In this study, reservoirs S1 and S2 were evaluated in terms of thickness, volume of shale, porosity, net-to-gross ratio, permeability, water saturation, and hydrocarbon saturation; the results are presented in Table 2, and Figure 4 depicts the relationship between the permeability and the total porosity used for the permeability estimation.

Table 2

Summary of petrophysical evaluation of reservoirs S1 and S2 in KO wells.

Well Name	Reservoir	Top depth (m)	Bottom depth (m)	Reservoir thickness (m)	PHIE	PERM (mD)	*N/G*	Hydrocarbon saturation
KO 1	**S1**	3556	3606	50	0.24	5651	0.92	0.60
	S2	3750	3847	97	0.21	4159	0.94	0.71
KO 2	**S1**	3537	3658	121	0.21	4804	0.89	0.39
	S2	3799	3901	102	0.20	3821	0.92	0.32
KO 3	**S1**	3580	3630	50	0.20	3775	0.89	N/A
	S2	3764	3870	106	0.18	2790	0.91	0.57
KO 4	**S1**	3559	3612	53	0.20	3542	0.95	0.51
	S2	3840	3924	84	0.20	3633	0.94	0.07

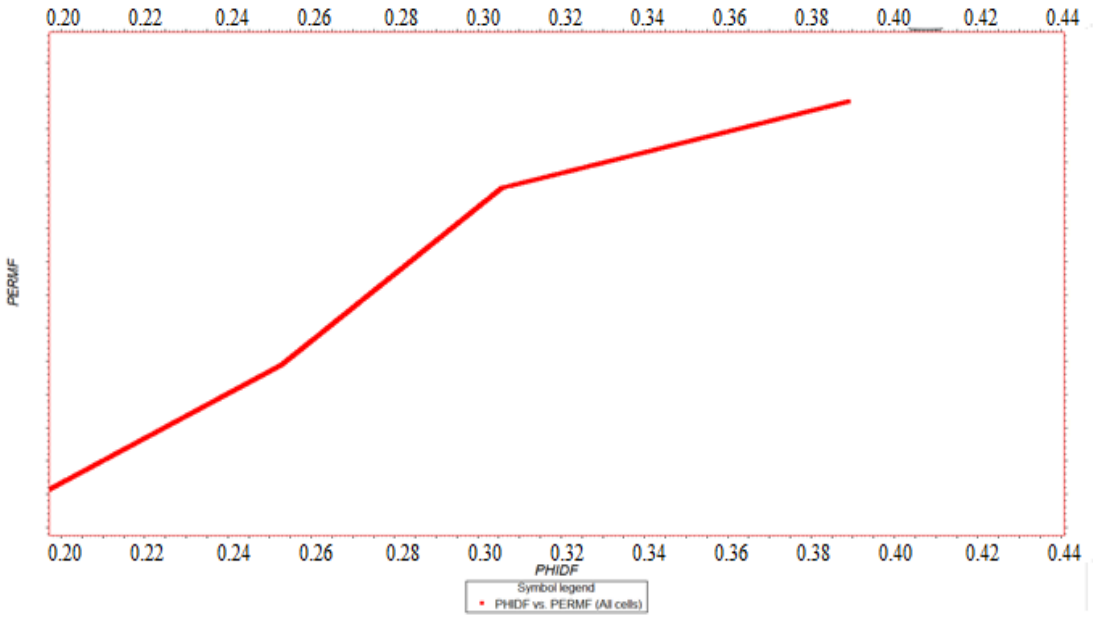

Figure 4

The cross-plot of the permeability versus the total porosity.

The thickness of reservoir S1 ranges from 50 to 121 m with a good porosity and permeability value of 20%–24% and 3542–5651 mD respectively. The water saturation (40%–61%) within this zone reflects a good hydrocarbon accumulation within the reservoir and a net-to-gross ratio ranging from 89%–95%.

The thickness of reservoir S2 ranges from 84 to 106 m with a good porosity and permeability value of 18%–21% and 2790–4159 mD respectively. The net-to-gross ratio ranges from 91%–94% similar to reservoir S1, while the water saturation (29%–68%) within this zone reflects a good hydrocarbon accumulation within the reservoir except at well KO 4 which is seen to be wet with a water saturation value of 93%.

3.5. Seismic to well tie

Following the creation of well tops in the reservoir zone, seismic to well tie was carried out using the check-shot data for well KO 4, the despiked sonic log (generated from the sonic log), and the density log.

The seismic to well tie involves two main processes: sonic calibration and the synthetic generation.

The sonic calibration was carried out using the check-shot and despiked sonic log of well KO 4, setting the datum as the marine datum since the seismic data were acquired swallow offshore. The sonic calibration track displays the knee point, the residual drift, the calibrated sonic, the sonic log, the quality control interval velocity, the input interval velocity, the input average velocity, and the input two-way travel time (TWT) picked. Further editing was carried on the knee point, and the calibrated time–depth relationship (TDR) generated in the sonic calibration was used for the synthetic generation alongside a deterministic wavelet in the zero phase. At the zero-phase wavelet, the maximum amplitude coincides with the spike of the reflector, and the pattern of the wavelet becomes symmetrical.

The synthetic generation displays the input log (density log), the reflection coefficient log (RC log), the left seismic reference, the synthetic seismogram, the right seismic reference, and the wavelet as illustrated in Figure 5.

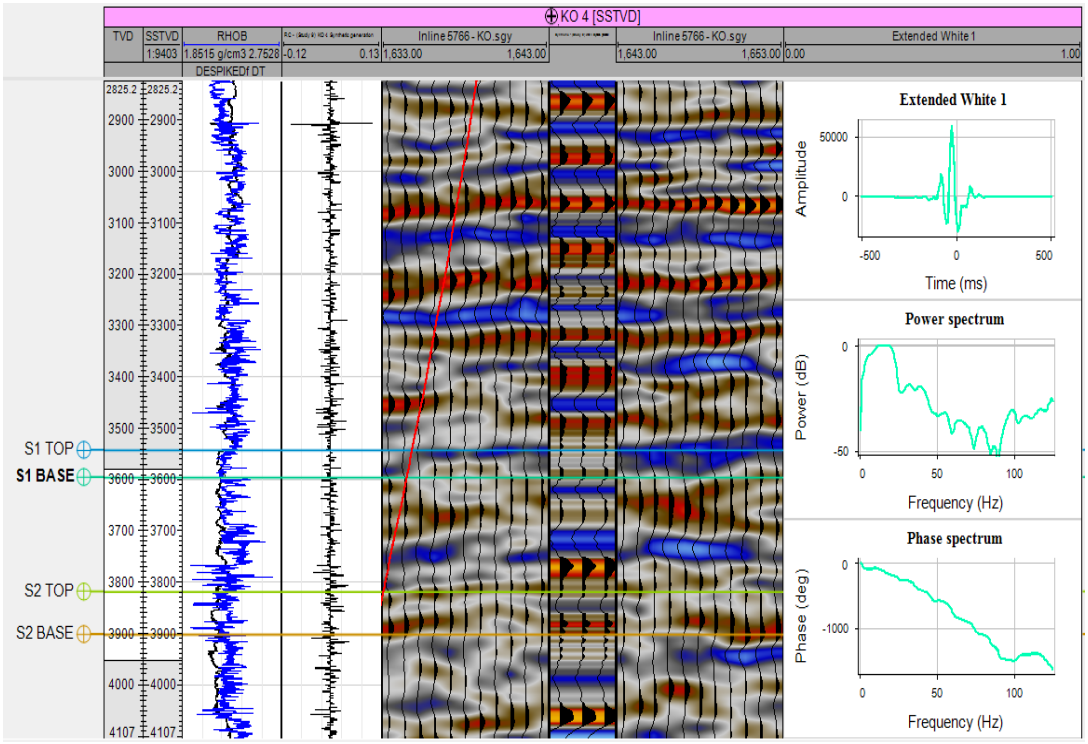

Figure 5

Synthetic seismogram generated from well KO 4.

From the seismic to well tie, we inferred that the seismic seismogram well matched the synthetic one. The peak of the seismic seismogram (red) correlates with the peak of the synthetic seismogram (red), while the trough of the seismic seismogram (blue) relates to the trough of the synthetic seismogram (blue). The well tops fall directly on a particular event to be interpreted.

3.6. Structural interpretation

The variance (edge method) and the cosine of the phase seismic volume and the surface attributes were respectively used for the structural mapping. The 3D time slice of the variance revealed that the field was faulted, while the faults were picked on the inlines at an interval of 10 m using the cosine of phase seismic attributes as seen in Figure 6. Fifteen fault sticks were mapped across the seismic section. It is seen in the fault framework that the wells are located within some of the interpreted faults, which suggests that the fault serves as a trap to prevent the further migration of hydrocarbon within the field. Normal faults, antithetic faults, and growth faults were identified within the field, which is typical of Niger Delta. The faults were labelled FT1 to FT15 and ran in the west–east direction.

A total of four horizons were mapped on the interpretation window of the inline and crossline using an interval of 10 m, two for each reservoir (the top and the base). The horizons were mapped based on the reflection point where the well tops fall on the seismic section. Most of the well tops fell in between a peak and a trough; thus, a zero-crossing signal feature was used for mapping alongside a seeded 2D auto-tracking tool for places with clear reflections and a manual interpretation tool for areas with chaotic reflections.

Mapping of horizons further revealed some of the structures on the section; structures such as a collapsed crest and rollover anticline (seen in Figure 7) were identified on the section, which is also very typical of the Niger Delta Agbada formation.

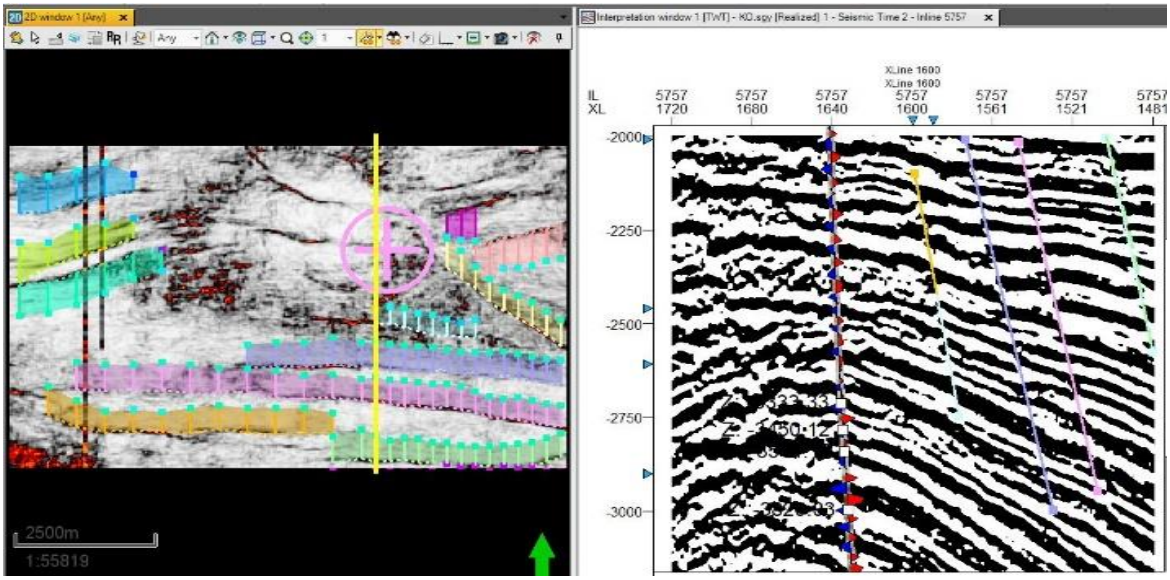

Figure 6

Fault picking on the interpretation window using the variance and cosine of phase attributes.

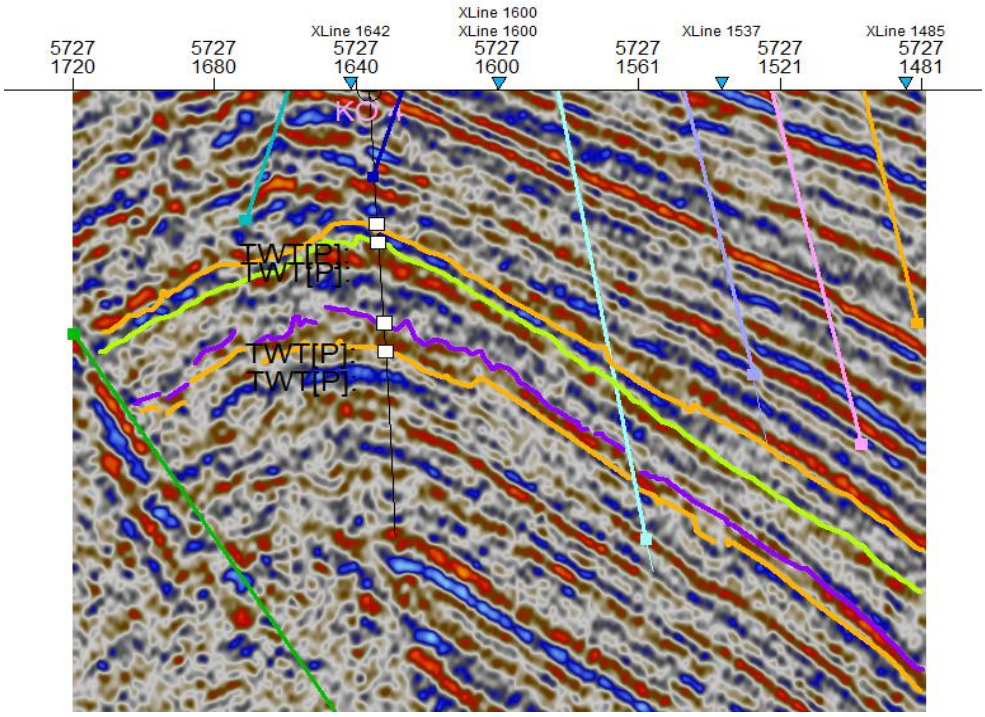

Figure 7

Horizon mapping across inline 5727.

3.7. Time to depth conversion

Faults and surface maps (generated from the horizons) which were in the TWT needed to be converted to true vertical depth (TVD) so that a proper depth estimation could be made. This conversion was performed by generating a relation between the depth and time plotting the check-shot data (depth against time) on well KO 4. The Petrel software function window (Figure 8) was used to plot the graph and generate a suitable equation; this equation was then used to convert each of the faults and surface maps to depth by employing the lookup function and calculator.

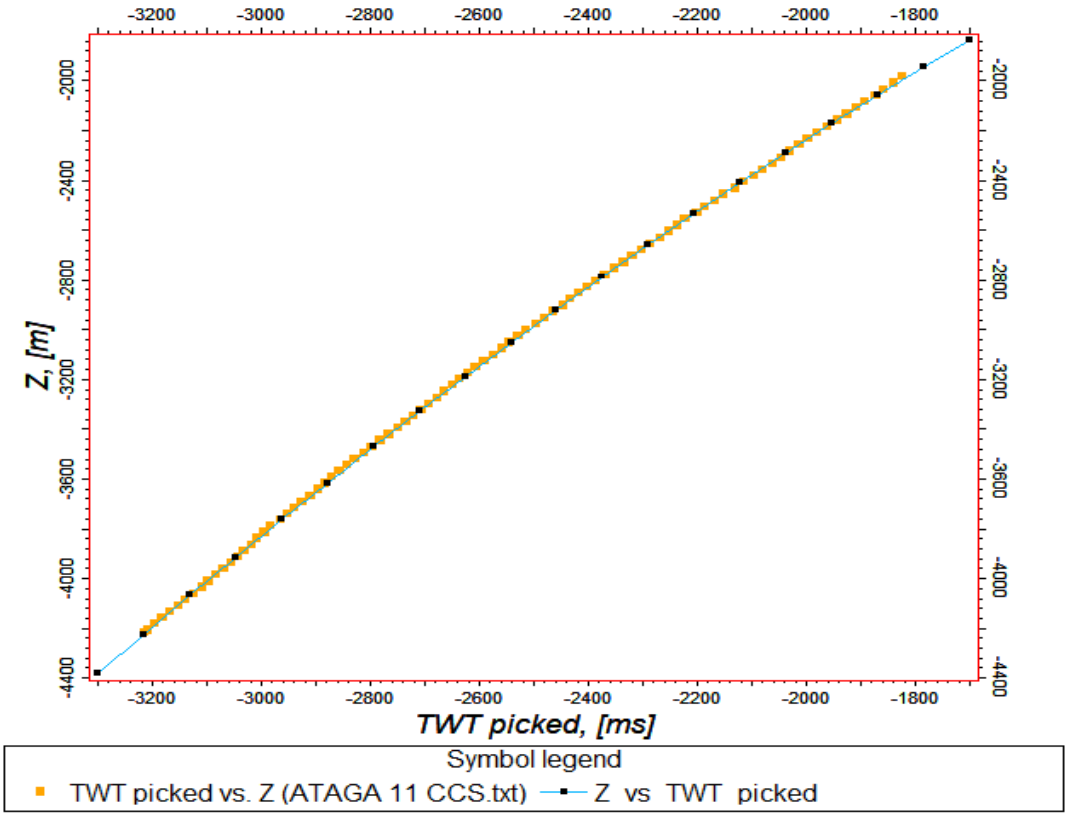

Figure 8

The relationship between the depth and time generated using check-shot data on well KO 4.

The relationship between the depth and time (Z versus TWT picked) generated from the least square method is given by:

$$y = -228.824 + 0.613864x - 0.0001954x^2 \quad (19)$$

4. Generation of structural maps

The structural time map was generated for reservoirs S1 and S2 (Figures 9 and 10 respectively) from the seismic horizon using the convergent interpolation method. Both reservoir maps were observed to have an anticlinal structure which favors the accumulation and retention of hydrocarbon provided that there is a seal.

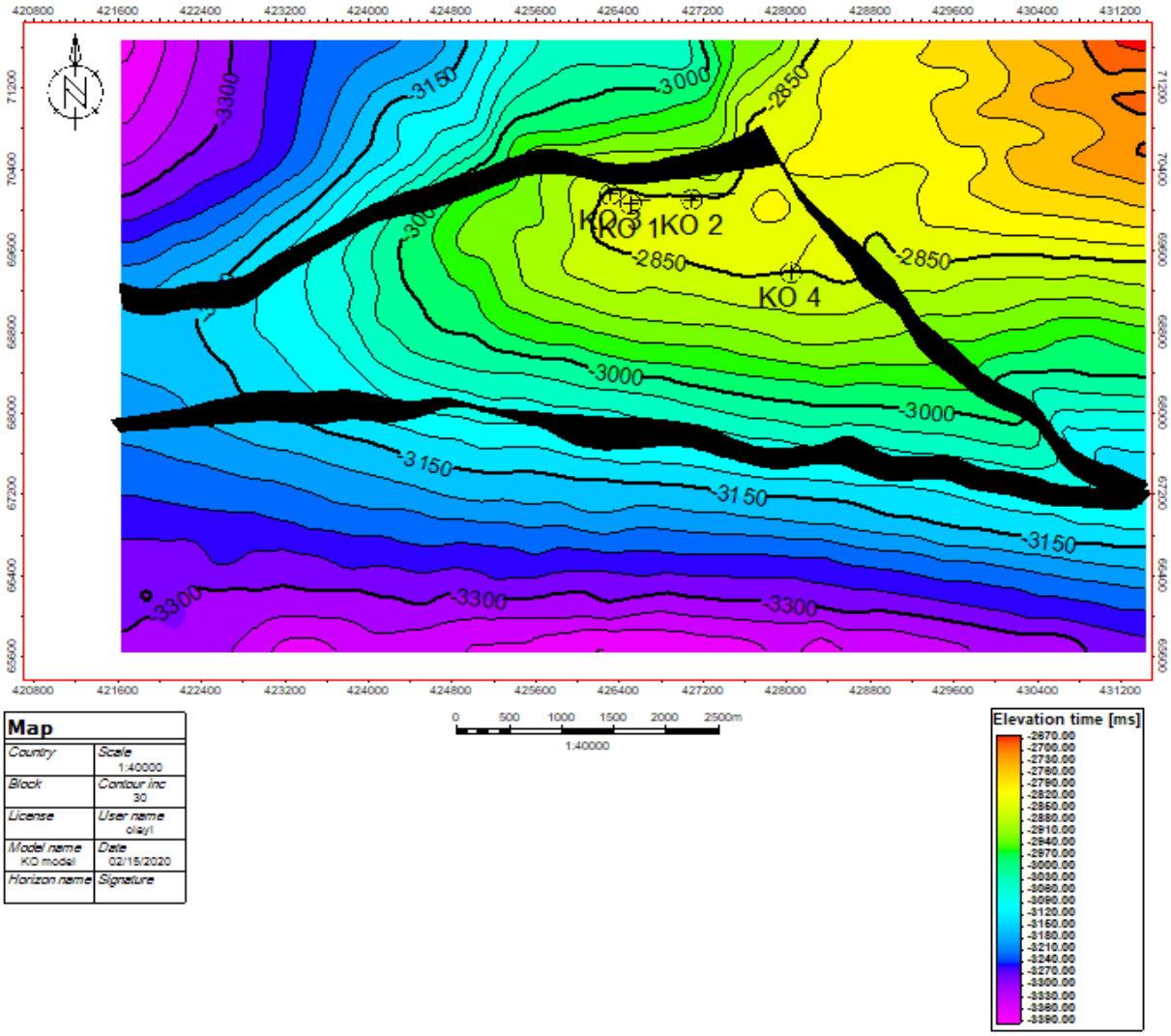

Figure 9

The time structural map of the top of reservoir S1.

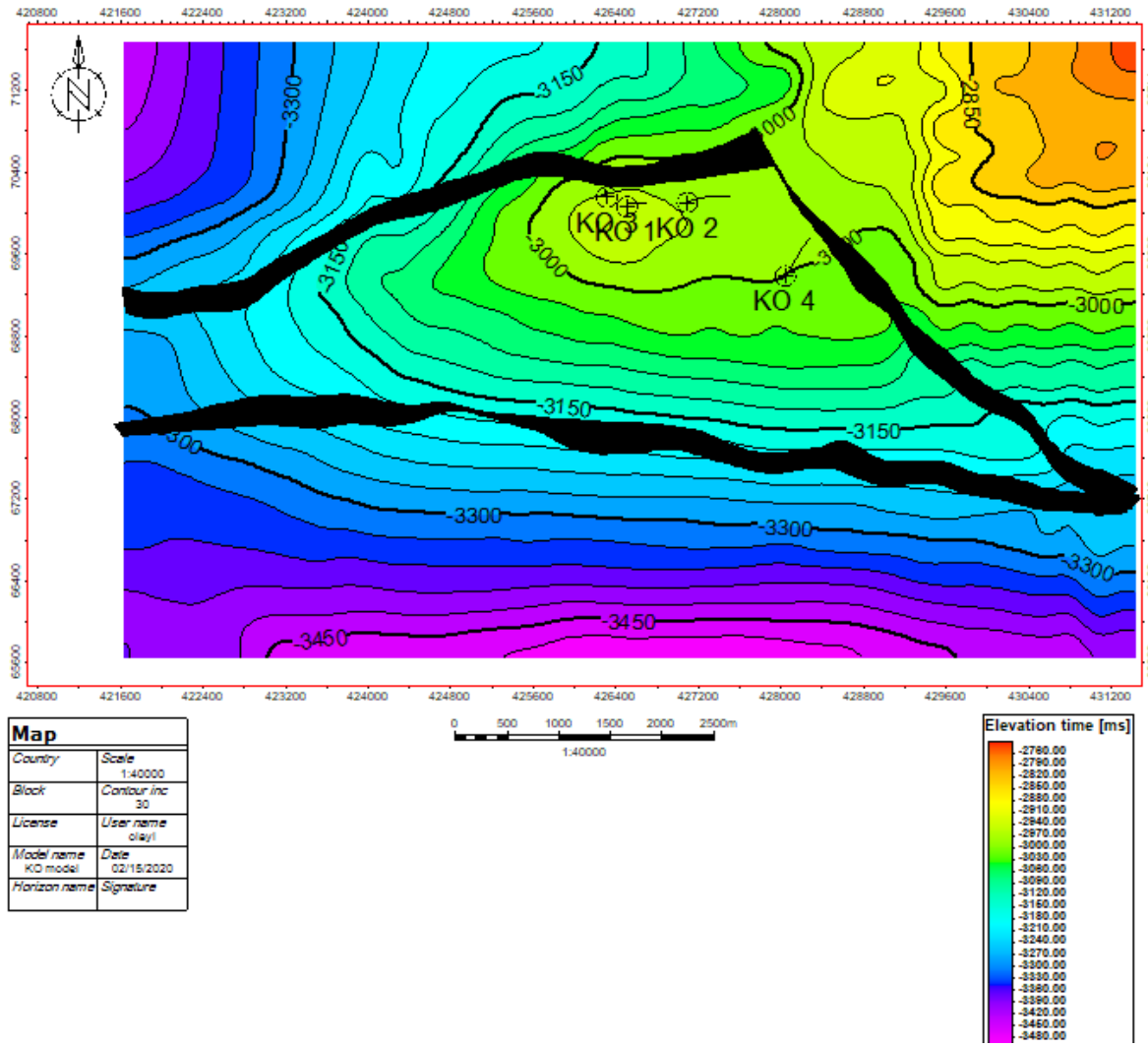

Figure 10

The time structural map of the top of reservoir S2.

The time map of reservoir S1 shows an elevation legend with the orange color indicating the shallowest part of the reservoir, while the purple color denoting the deepest part of the reservoir. The contoured time value ranges from 2700 to 3420 ms.

Similarly, the time map of reservoir S2 displays an elevation legend with the orange color indicating the shallowest part of the reservoir, while the purple color denoting the deepest part of the reservoir. The contoured time value ranges from 2760 to 3550 ms.

According to the depth maps seen in Figures 11 and 12, there was good agreement between the structural time maps and the structural depth maps, indicating that the depth time equation used for converting the time map was suitable. The depth of the reservoirs was within a contour of 3330 to 4350 m. The structural depth maps also had an anticlinal structure with the major faults oriented in the same direction as that of the major faults on the time maps. The structural depth maps had fault-assisted closure; these faults act as a seal to prevent the further migration of hydrocarbons.

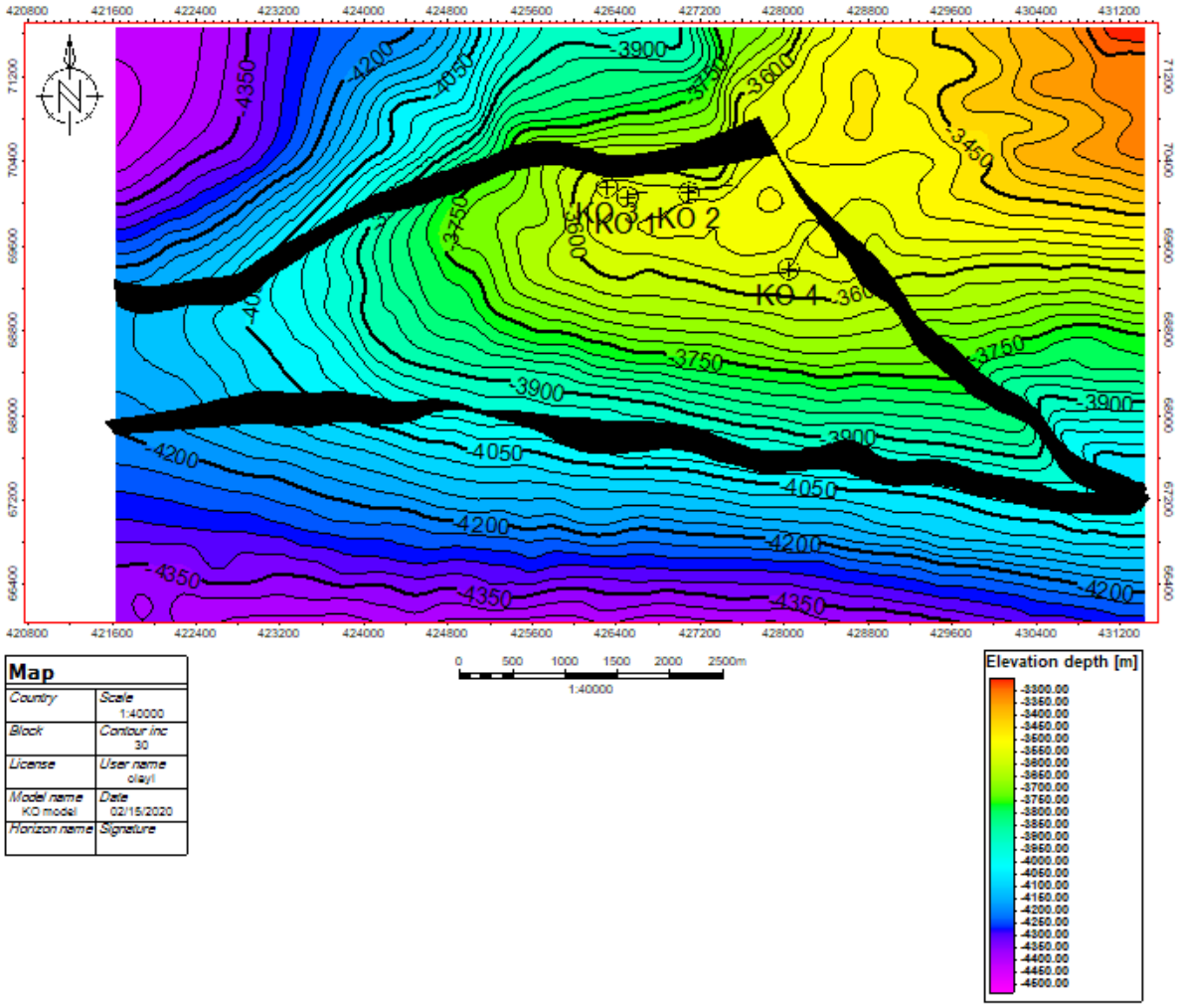

Figure 11

The depth structural map of the top of reservoir S1.

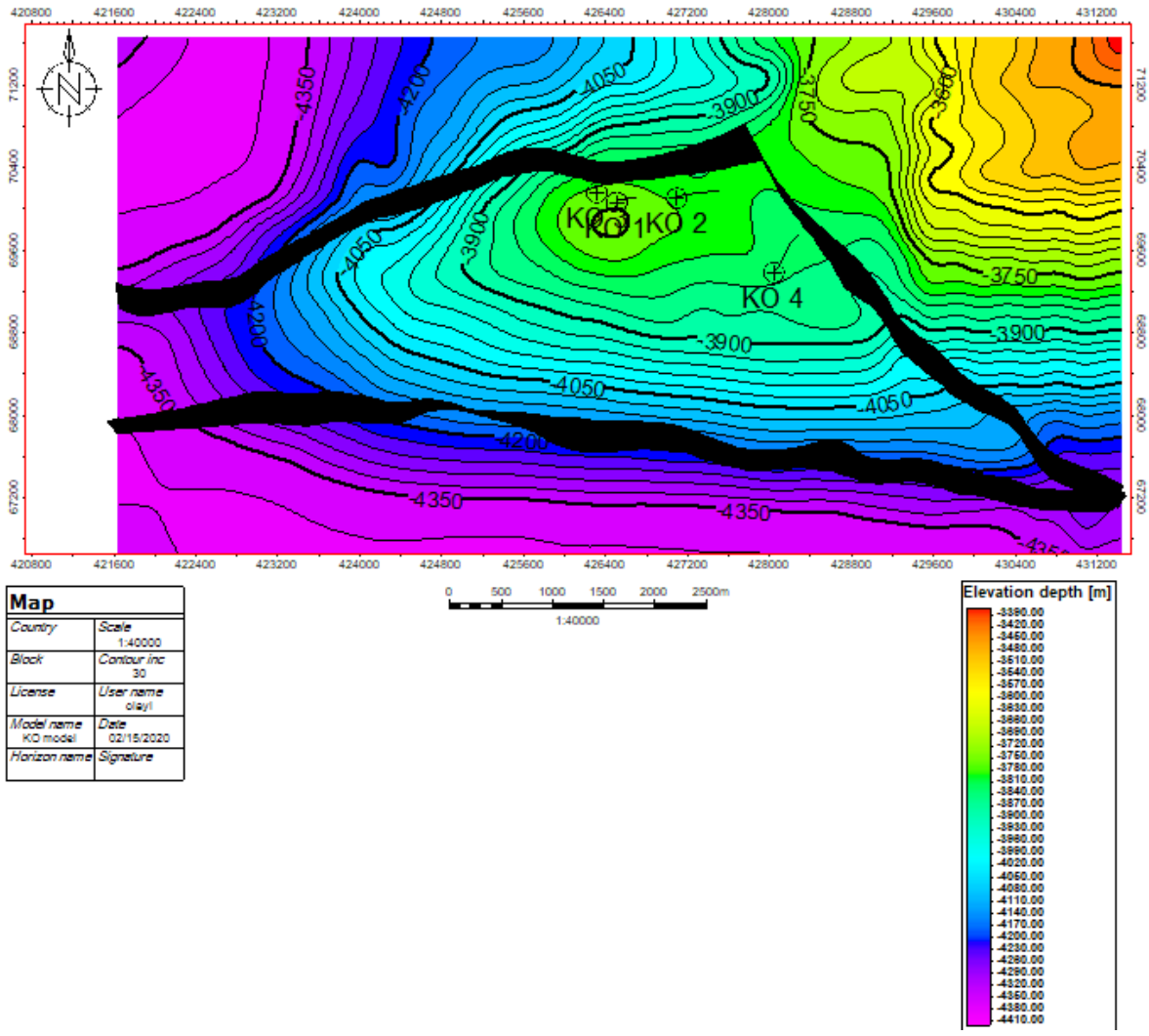

Figure 12

The depth structural map of the top of reservoir S2.

4.1. Attributes analyses

In order to confirm the presence of hydrocarbon in the identified structures and to identify stratigraphic traps which are not shown on the depth structure maps, attributes analyses were carried out (Abe and Olowokere, 2013). Root mean square (RMS) amplitude attributes computed for the horizon tops revealed high amplitude areas as seen in Figures 13 and 14. Low amplitude areas were also spotted around well KO 4 through the RMS amplitude time slice at a *Z* value of –3084.00 (Figure 15) close to the top of reservoir S2, affirming the wettest area spotted in the resistivity log and the high-water saturation calculated by the petrophysical evaluation.

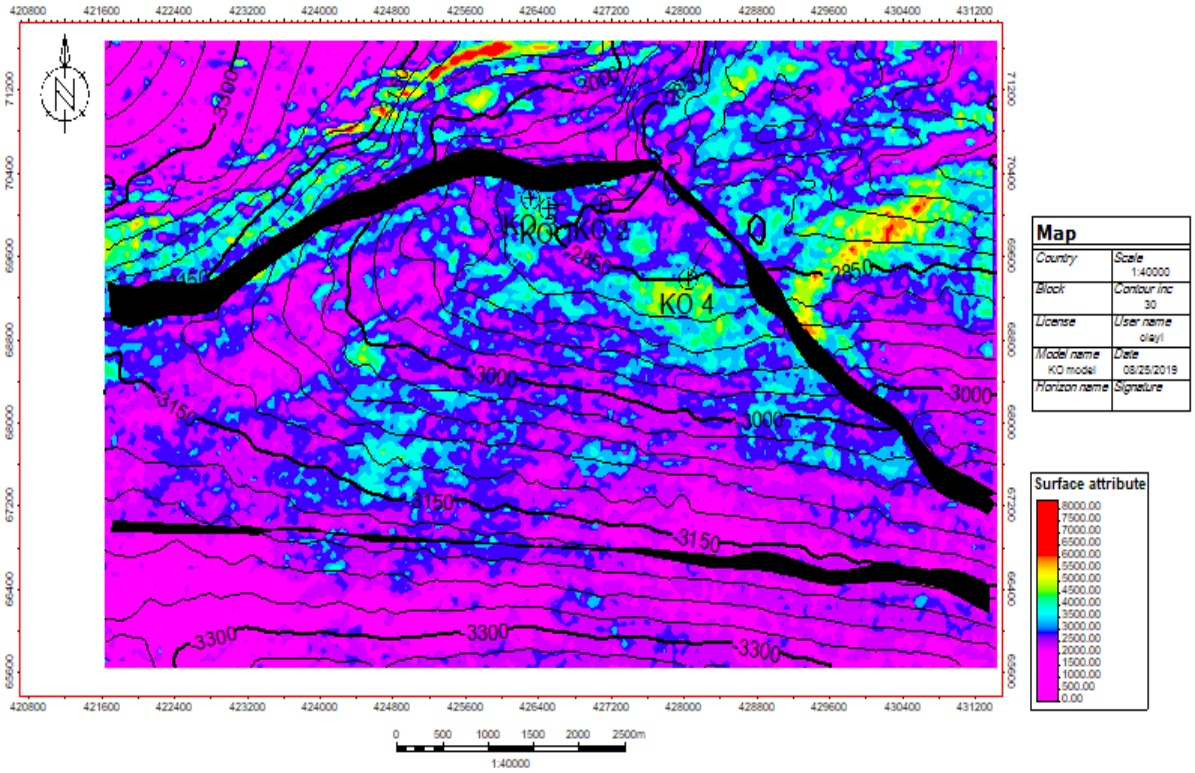

Figure 13

The RMS amplitude map of reservoir S1.

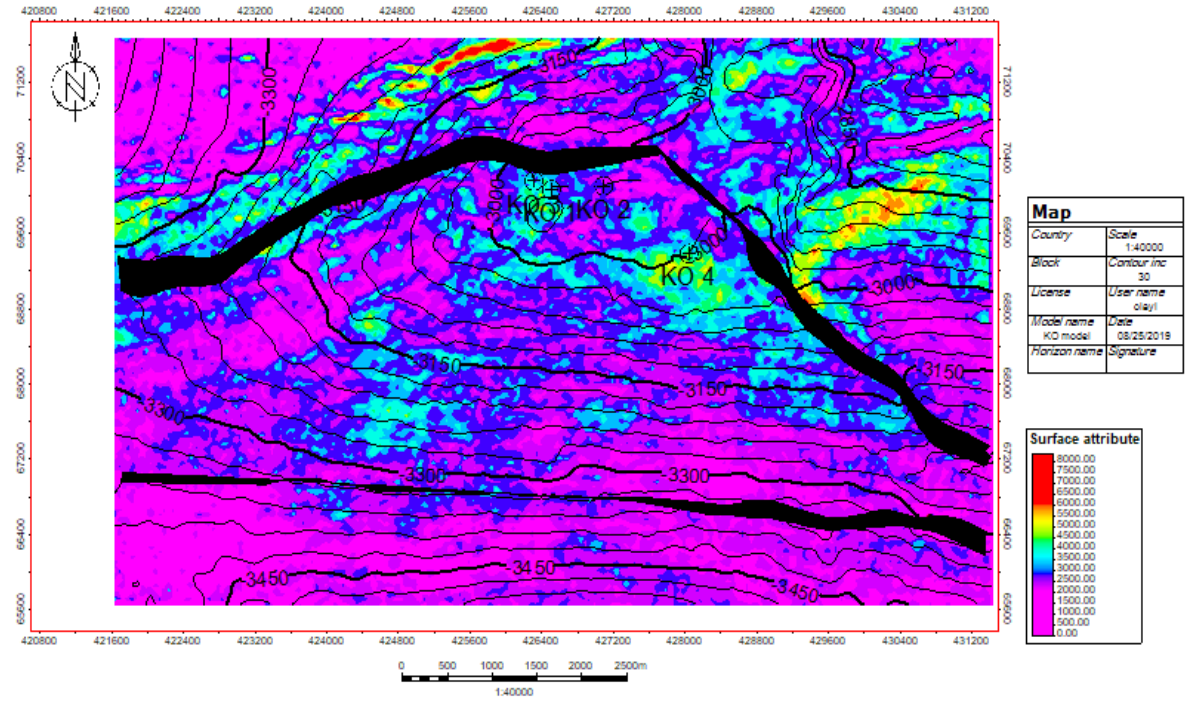

Figure 14

The RMS amplitude map of reservoir S2.

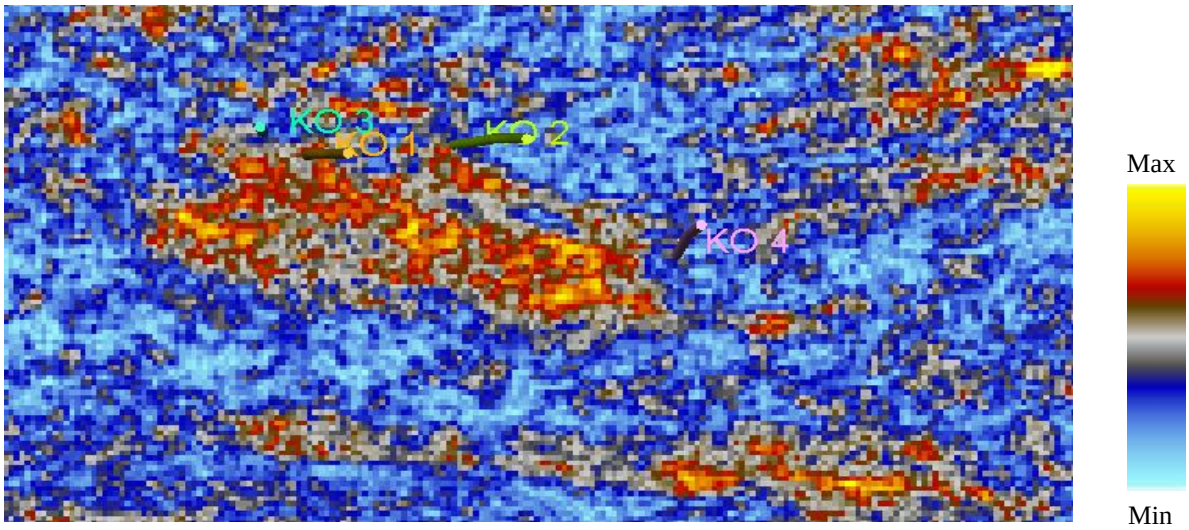

Figure 15

The RMS amplitude extraction close to the top of horizon S2 at Z = –3084.00.

The variance edge seismic attribute (Figure 16) correlates well with the faults and fractures within the study area. The signatures of the faults were enhanced through calculating the variance within the seismic data volume with an edge enhancement option, thereby enabling the mapping across discontinuities within the data.

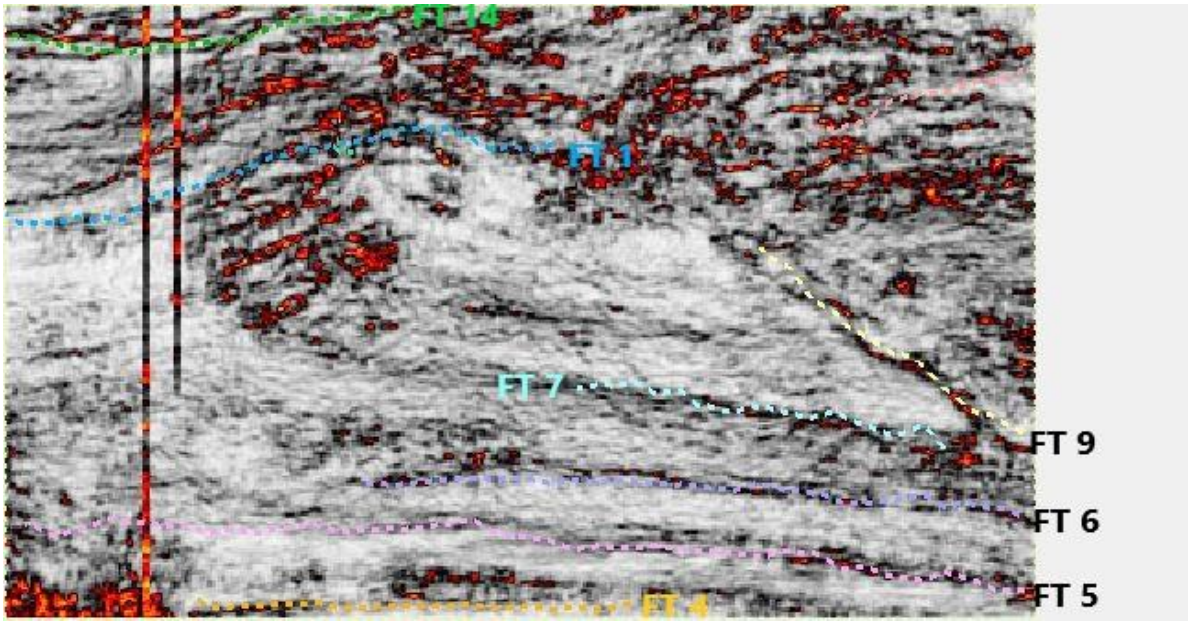

Figure 16

The time slice of variance attributes displaying clearly some of the mapped faults.

4.2. Static reservoir model

A structural framework built in the depth domain was created at the first stage of the structural modeling. Fault framework modeling and horizon modeling were also established. The fault framework model includes the seven faults that impact the reservoirs, including FT1, FT6, FT7, FT 9, FT10, FT11, and FT14, while the horizon model consists of all the four structural maps in depth, well tops, and the isochore thickness maps obtained from the well tops.

Figure 17 illustrates the pillar gridding of the faults and the skeletal framework of the model. The skeletal framework of the reservoir has 98 × 63 nodes and 97 × 62 cells, indicating the total number of 2D nodes of 6174 and the total number of 2D cells of 6014.

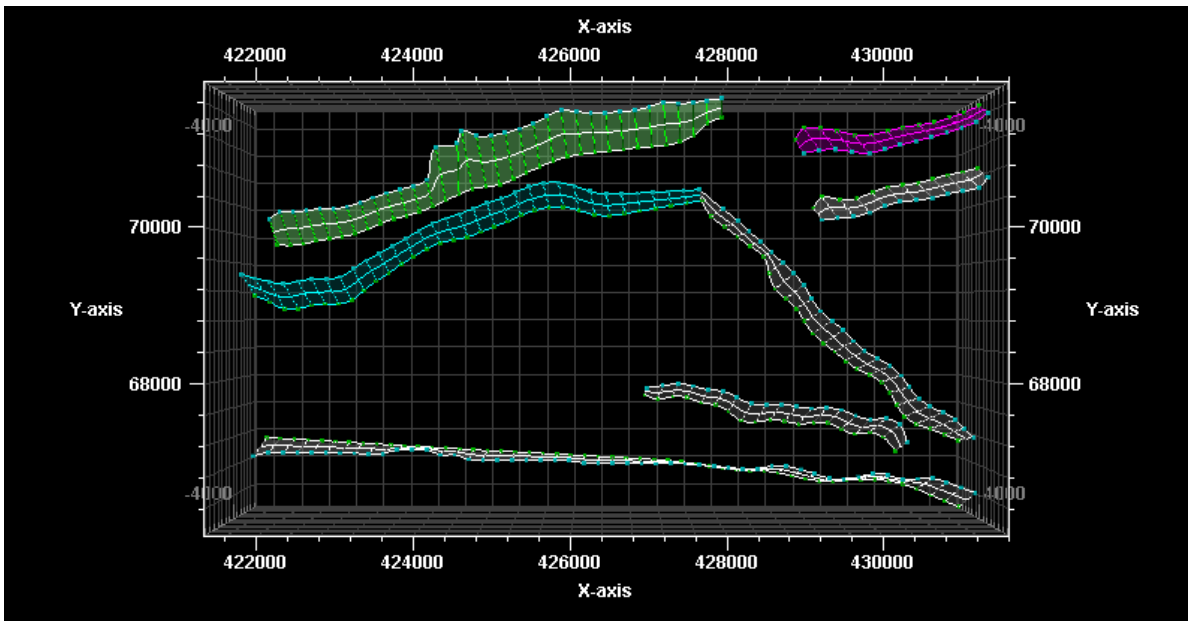

Figure 17

The above view of the pillar gridding.

4.3. Facies model

A facies model was created using the upscaled facies log. The results of the lithofacies model of both reservoirs can be seen in Figure 18. The model shows a high sand-to-shale proportion conforming to the geologic knowledge of most reservoirs in Niger Delta and consists of a total number of 42098 grid cells. This lithofacies model was utilized to constrain the distribution of the petrophysical properties.

a)

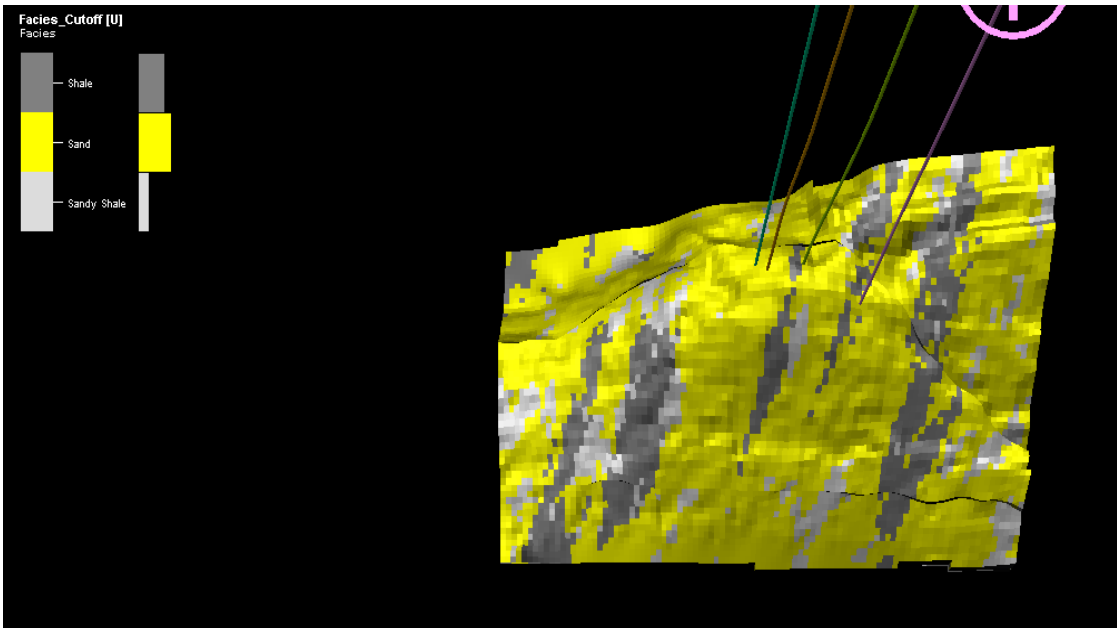

b)

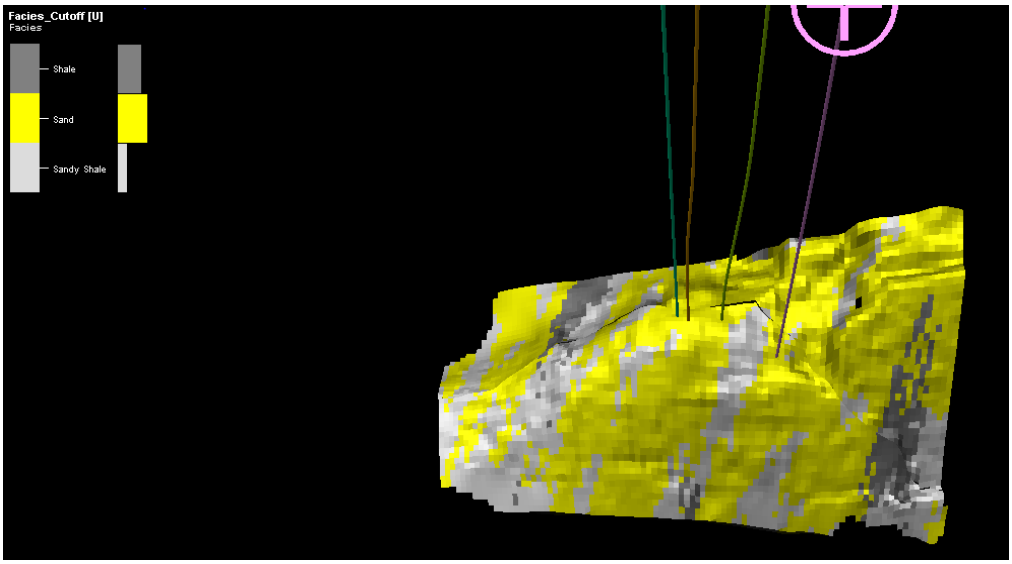

Figure 18(b)

a) The facies model of reservoir S1 and b) the facies model of reservoir S2.

5. Petrophysical model

5.1. Porosity model

The effective porosity of reservoirs S1 and S2 (see Figure 19) was modeled using the upscaled porosity log generated during the petrophysical evaluation.

a)

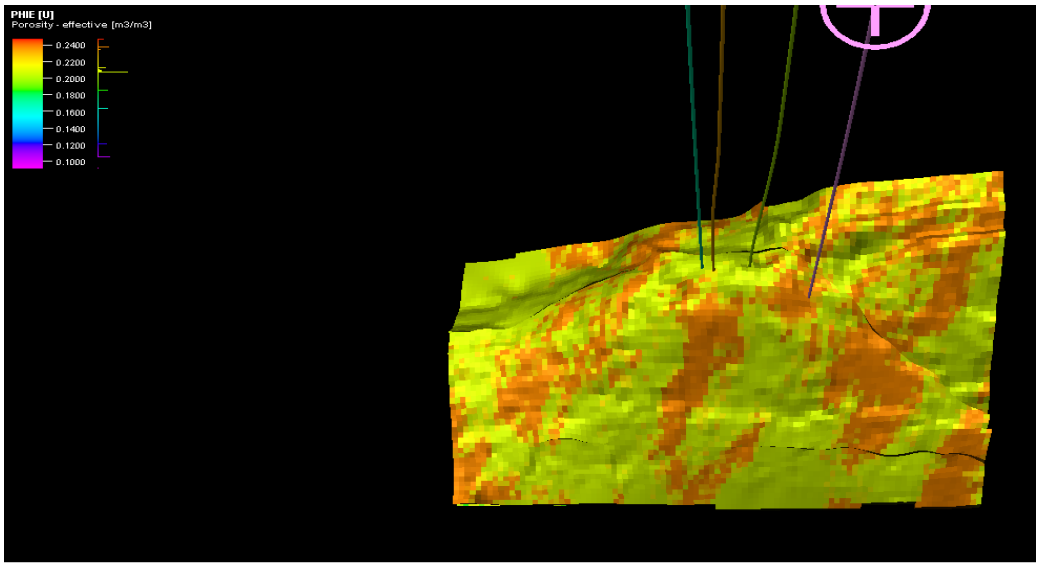

b)

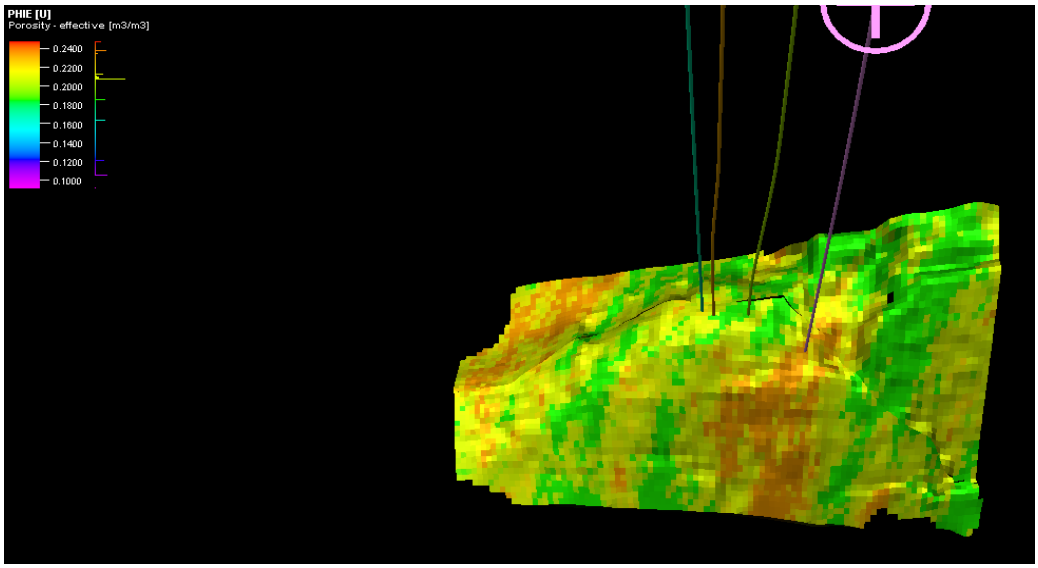

Figure 19

a) The effective porosity model of reservoir S1 and b) the effective porosity model of reservoir S2.

The effective porosity presents the volume of the interconnected pores within the reservoir, that is, it determines the volume of the pores contributing to the production of the fluid within the reservoir. The effective porosity model shows that reservoir S1 has a minimum effective porosity of 0.20 and a maximum effective porosity of 0.24. The average effective porosity within this reservoir is 0.213, indicating that the pores within the reservoir are well connected.

Similarly, reservoir S2 has a minimum effective porosity of 0.18 and a maximum effective porosity of 0.24. The average effective porosity within this reservoir is 0.198, indicating that the reservoir is very porous.

5.2. Permeability model

The permeability model demonstrates that reservoir S1 has a minimum permeability of 5303 mD and a maximum permeability of 7528.8 mD as seen in Figure 20. The average permeability of this reservoir is 6224.5 mD, implying that the reservoir is permeable.

a)

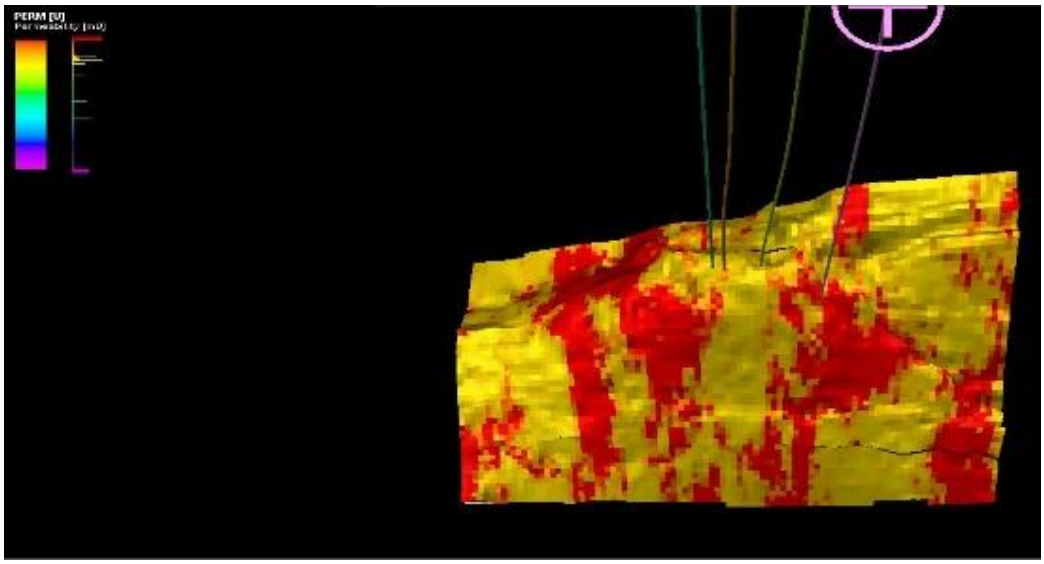

b)

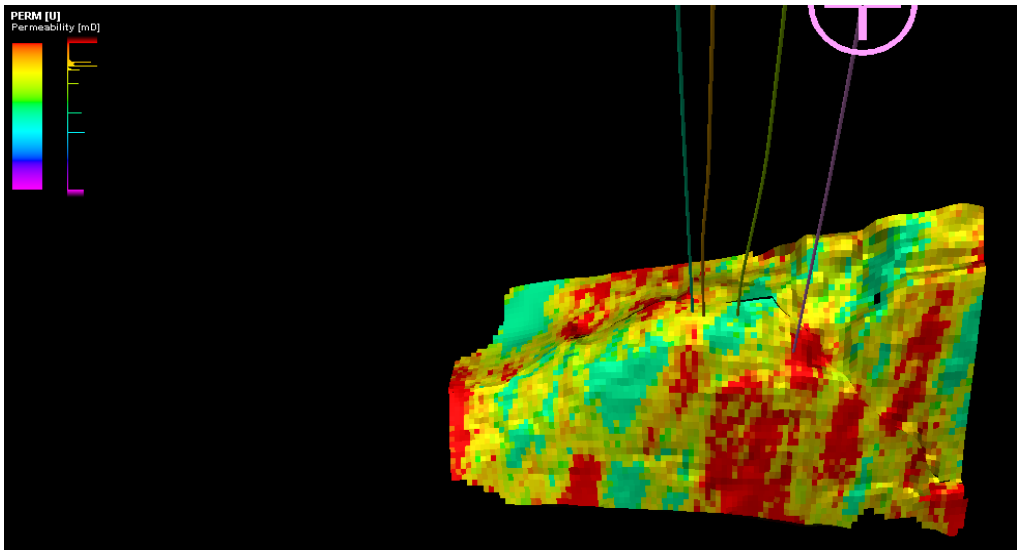

Figure 20

a) The permeability model of reservoir S1 and b) the permeability model of reservoir S2.

Reservoir S2 has a minimum permeability of 4631.8 mD and a maximum permeability of 5928.6 mD as seen in Figure 20. The average permeability of this reservoir is 5419 mD, indicating that the fluids can move properly within the pores of the reservoir.

5.3. Hydrocarbon saturation model

The hydrocarbon saturation models of the two reservoirs were developed as displayed in Figure 21. These models help obtain the distribution of hydrocarbon and water within the reservoirs. The average hydrocarbon saturation of reservoir S1 is 0.50, while reservoir S2 has a hydrocarbon saturation of 0.42 due to the presence of wet well KO 4.

a)

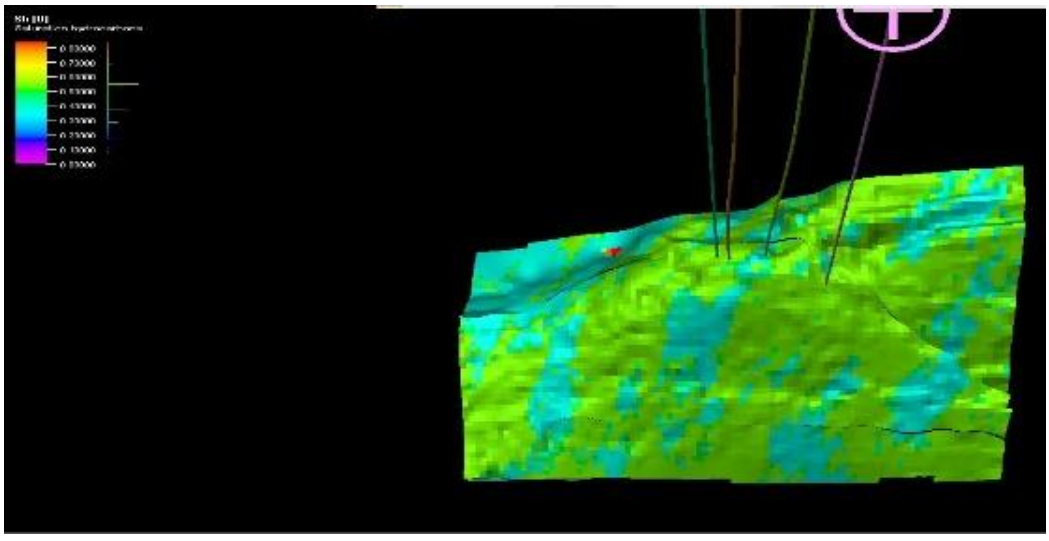

b)

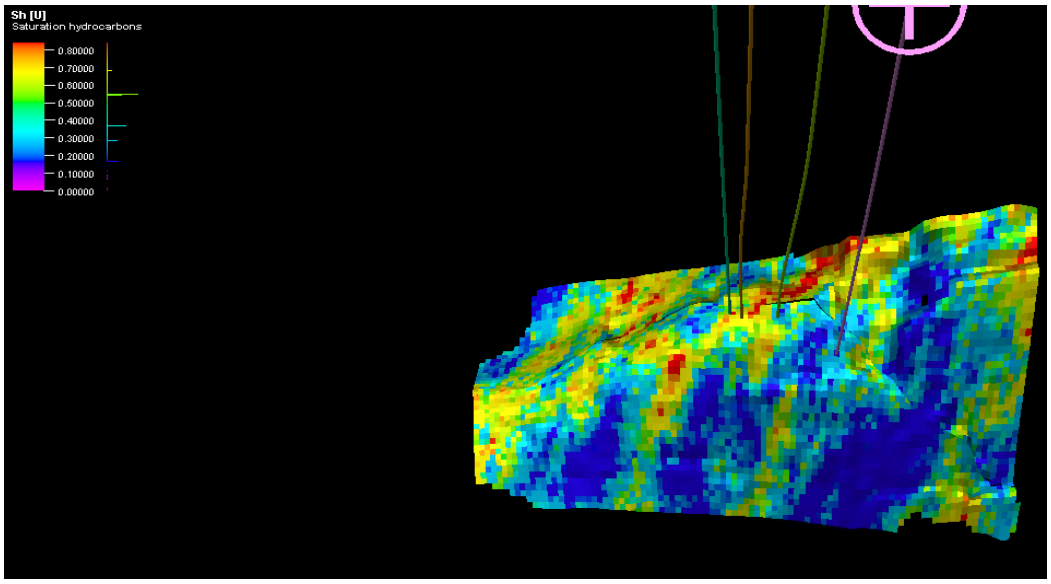

Figure 21

a) The hydrocarbon saturation model of reservoir S1 and b) the hydrocarbon saturation model of reservoir S2.

5.4. Fluid contacts

The fluids of reservoirs S1 and S2 are gas, oil, and water. Figure 22 depicts the gas–oil contact (GOC) and oil–water contact (OWC) in the reservoirs. Reservoirs S1 and S2 predominately contain gas and water with little oil. The gas and oil reserves occupy the red and green parts of the reservoir contact maps respectively, while water is seen in the blue section of the reservoir contact maps.

a)

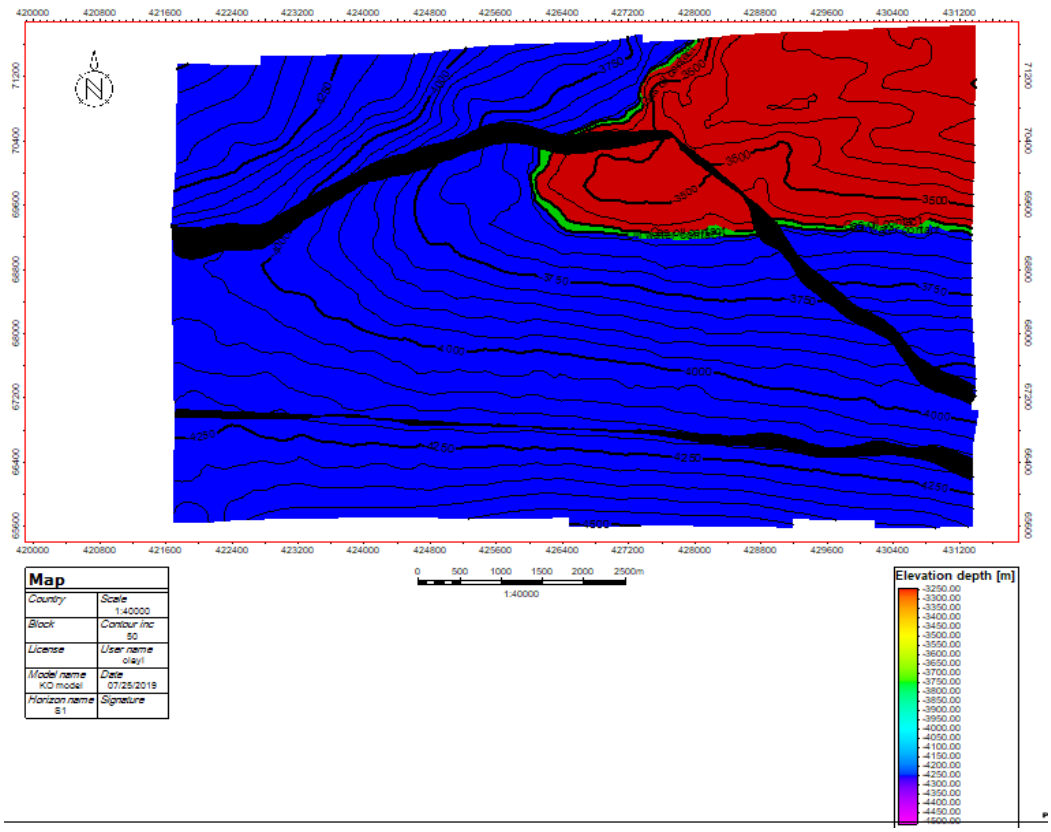

b)

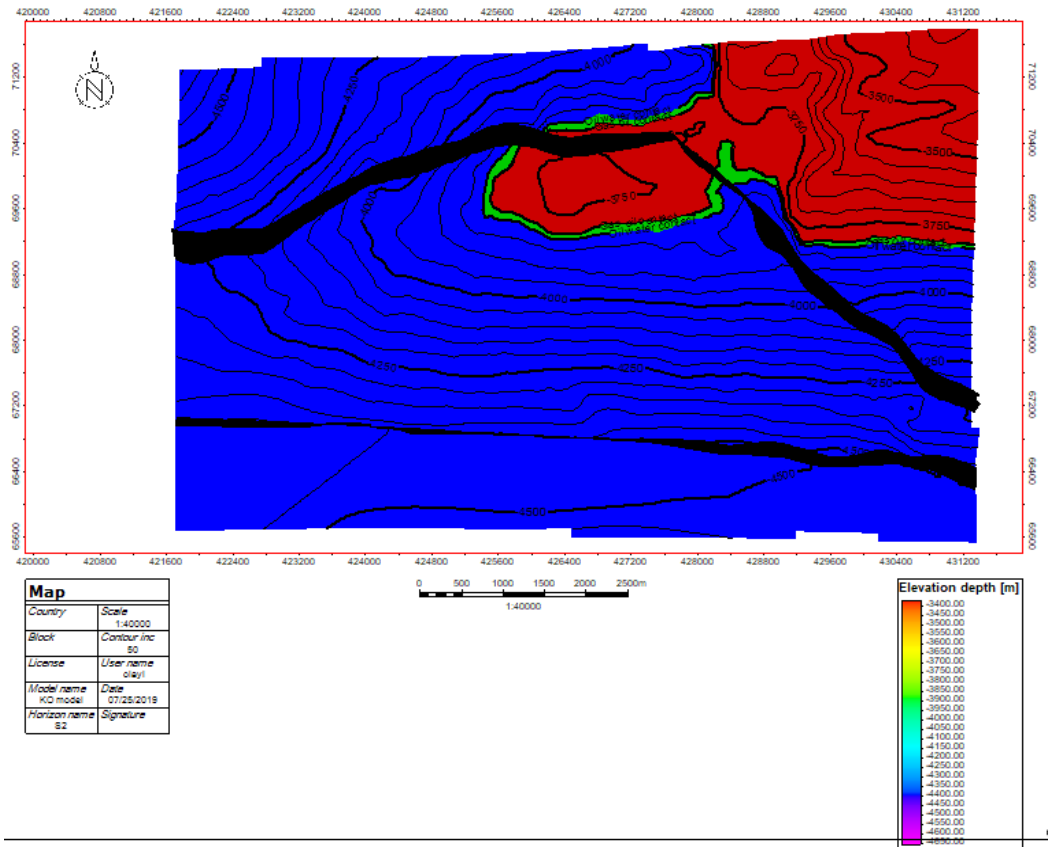

Figure 22

a) The fluid contact map of reservoir S1 and b) the fluid contact map of reservoir S2.

5.5. Volumetric assessment

Using the model-based volumetric calculation, the stock tank oil initially in place (STOIIP) and gas initially in place (GIIP) of reservoir S1 were estimated to be 35 mmbbl and 63294 mmcf respectively. Moreover, the STOIIP and GIIP of reservoir S2 were estimated at 70 mmbbl and 26714 mmcf respectively .

The model was divided into three segments; the lowest part of the segment, i.e. segment 3, was completely saturated with water, while segments 1 and 2 were estimated to have a varying amount of hydrocarbon and water as presented in Table 3.

Table 3

The estimation results of reservoirs S1 and S2.

	Bulk volume ($\times 10^6$ m^3)	**Net volume ($\times 10^6$ m^3)**	**Pore volume ($\times 10^6$ m^3)**	**HCPV oil ($\times 10^6$ m^3)**	**HCPV gas ($\times 10^6$ m^3)**	**STOIIP ($\times 10^6$ m^3)**	**GIIP ($\times 10^6$ m^3)**	**Recoverable oil ($\times 10^6$ m^3)**	**Recoverable gas ($\times 10^6$ m^3)**
Case	1517	1387	296	126	81	104	90008	104	90008
				Zones					
S1 TOP- S1 BASE	995	906	202	84	57	70	63294	70	63294
S2 TOP-S2 BASE	522	481	94	42	24	35	26714	35	26714
				Segments/Regions					

	Bulk volume ($\times 10^6$ m^3)	**Net volume ($\times 10^6$ m^3)**	**Pore volume ($\times 10^6$ m^3)**	**HCPV oil ($\times 10^6$ m^3)**	**HCPV gas ($\times 10^6$ m^3)**	**STOIIP ($\times 10^6$ m^3)**	**GIIP ($\times 10^6$ m^3)**	**Recoverable oil ($\times 10^6$ m^3)**	**Recoverable gas ($\times 10^6$ m^3)**
Segment 1	287	262	55	26	13	21	13994	21	13994
Segment 2	1231	1125	241	100	68	83	76013	83	76013
Segment 3	0	0	0	0	0	0	0	0	0

6. Conclusions

This research demonstrates the versatility of using 3D seismic and well log data for structural interpretation, petrophysical analysis, reservoir modeling, and reservoir characterization. The reservoir characterization of KO field reveals the two major lithological units in this area: the sand and the shale. The lithofacies analysis indicates that both reservoirs are of good and moderate-quality, which supports the petrophysical properties in terms of effective porosity, permeability, net-to-gross ratio, and hydrocarbon saturation.

The RMS amplitude from the horizon reveals high amplitude areas on and around the structural highs which coincide with the locations where wells KO 1, KO 2, KO 3, and KO 4 were already drilled, thereby validating the earlier interpretations that led to the drilling of the well. The cosine of phase and variance edge attributes enhanced the visibility of the faults and other structural features in the field, which assisted with the interpretation. An anticlinal structure was spotted in the center of the surfaces with the major faults running across the field. The structural disposition of the four horizons mapped greatly favored the accumulation of hydrocarbon coupled with the good reservoir parameters obtained from the well. The accumulation and trapping of hydrocarbon in this field are fault-dependent.

The geological model constructed provided an insight into how facies and petrophysics properties are distributed spatially within the reservoirs. We suggest that more wells should be drilled within the field to provide more input data on the static models since this will increase the confidence level of the output of our models and will enable us to explore other potential prospects in the field. A complete data set, including formation volume factor for oil and gas, pressure data, and the recovery factor evaluated for the field should be provided for students to achieve a good, quality interpretation and accurate STOIIP and GIIP values. This will help avoid the overestimation or underestimation of the hydrocarbon in place. One remaining question will be ascertaining the consistency of the model and its ability to reproduce the observed reservoir performance.

Nomenclature

GIIP	Gas initially in place
HCPV	Hydrocarbon pore volume
KO 1	KO well 1
KO 2	KO well 2
KO 3	KO well 3
KO 4	KO well 4
PERM	Permeability
PHIE	Effective porosity
Sat	Saturation
STOIIP	Stock tank oil initially in place
TWT	Two-Way Traveltime
TVD	True Vertical Depth
RMS	Root Mean Square

References

Abe, S. J. and Olowokere, M. T., Reservoir Characterization and Formation Evaluation of Some Part of Niger Delta Using 3D Seismic and Well Log Data, Research Journal in Engineering and Applied Sciences, Vol. 2, No. 4, p. 304–307,2013.

Archie, G. E., The Electrical Resistivity Log as an Aid in Determining Some Reservoir Characteristics, Petroleum Transactions of The AIME, Vo.146, p. 54–62, 1942.

Cosentino, L., Integrated Reservoir Studies, Editions Technip, Paris, 25 P., 2001.

Doust, H., Omatsola, E., Niger Delta, in, Edwards, J. D., and Santogrossi, P.A., Eds., Divergent/Passive Margin Basins, AAPG Memoir 48: Tulsa, American Association of Petroleum Geologists, p. 239–248, 1990.

Ejedawe, J. E., Coker, S. J. L., Lambert-Aikhionbare, D. O., Alofe, K. B., and Adoh, F. O., Evolution of Oil-generative Window and Oil and Gas Occurrence in Tertiary Niger Delta Basin, American Association of Petroleum Geologists, Vol. 68, p. 1744–1751, 1984.

Herrera, V. M., Russell, B., and Flores, A., Neural Networks in Reservoir Characterization, The Leading Edge, Vol. 25, No. 4, p. 402–411, 2006, Doi: 10.1190/1.2193208

Lawrence S. R., Monday S., Bray R., Regional Geology and Geophysics of The Eastern Gulf of Guinea (Niger Delta To Rio Muni), Lead Edge, Vol. 21, p. 1112–1117, 2002.

Mickaele Le R., Brigitte D., Olivier L., Integrated Reservoir Characterization and Modeling, 2014.

Partyka, G., Gridley, J., and Lopez, J., Interpretational Applications of Spectral Decomposition in Reservoir Characterization: The Leading Edge, Vol. 18, No. 3, p. 353–360, 1999.

Reijers, T. J. A., Selected Chapters on Geology: with Notes on Sedimentary Geology, Sequence Stratigraphy and Three Case Studies and a Field Guide Warri, Nigeria: S.P.D.C. Corporate Reprographic Services, p. 197, 1996.

Schlumberger, Log Interpretation, Principles and Application: Schlumberger Wireline and Testing, Houston, Texas, p. 21–89, 1989.

Schlumberger, Seismic-to-Simulation Software: Petrel Introduction Course, Houston, Texas, p. 101–15, 2007.

Tuttle, L. W. Michele, Ronald, R., Charpentier, and Michael, E., Brownfield, The Niger Delta Petroleum System: Niger Delta Province, Nigeria Cameroon, and Equatorial Guinea, Africa: Open-file Report 99-50-H, 1999.

Wyllie, M. R. J. and Rose W. D., Some Theoretical Considerations Related to the Quantitative Evaluation of The Physical Characterization of Reservoir Rock from Electric Log Data, Trans. AIME, Vol. 189, p. 105, 1950, Doi: 10.2118/950105-G.